Probing the Complex Ion Structure in Liquid Carbon at 100 GPa

D. Kraus,[1] J. Vorberger,[2] D. O. Gericke,[3] V. Bagnoud,[4] A. Blažević,[4] W. Cayzac,[1,5] A. Frank,[6] G. Gregori,[7] A. Ortner,[1] A. Otten,[1] F. Roth,[1] G. Schaumann,[1] D. Schumacher,[1] K. Siegenthaler,[1] F. Wagner,[1] K. Wünsch,[3,8] and M. Roth[1]

[1]*Institut für Kernphysik, Technische Universität Darmstadt, Schlossgartenstraße 9, 64289 Darmstadt, Germany*
[2]*Max-Planck-Institut für Physik komplexer Systeme, Nöthnitzer Straße 38, 01187 Dresden, Germany*
[3]*Centre for Fusion, Space and Astrophysics, Department of Physics, University of Warwick, Coventry CV4 7AL, United Kingdom*
[4]*GSI Helmholtzzentrum für Schwerionenforschung GmbH, Planckstraße 1, 64291 Darmstadt, Germany*
[5]*Université de Bordeaux-CEA-CNRS CELIA UMR 5107, 351 Cours de la Libération, 33405 Talence, France*
[6]*Helmholtz-Institut Jena, Fröbelstieg 3, 07743 Jena, Germany*
[7]*Department of Physics, University of Oxford, Parks Road, Oxford OX1 3PU, United Kingdom*
[8]*Tessella, 26 The Quadrant, Abingdon OX14 3YS, United Kingdom*

(Received 19 June 2013; published 16 December 2013)

We present the first direct experimental test of the complex ion structure in liquid carbon at pressures around 100 GPa, using spectrally resolved x-ray scattering from shock-compressed graphite samples. Our results confirm the structure predicted by *ab initio* quantum simulations and demonstrate the importance of chemical bonds at extreme conditions similar to those found in the interiors of giant planets. The evidence presented here thus provides a firmer ground for modeling the evolution and current structure of carbon-bearing icy giants like Neptune, Uranus, and a number of extrasolar planets.

DOI: 10.1103/PhysRevLett.111.255501 PACS numbers: 62.50.−p, 61.05.cf, 81.05.U−, 81.40.Vw

As one of the most abundant elements, carbon plays a crucial role in planetary physics. Liquid carbon is predicted to exist as a pure phase in the interior of giant planets since methane, which is highly abundant on the surface of, e.g., Neptune and Uranus, is believed to dissociate under pressures above 100 GPa and carbon may phase separate from hydrogen [1–4]. Moreover, the recent discovery of extrasolar planets, which may consist of up to 50% of carbon, further raises the need to understand carbon under extreme conditions [5]. Carbon at even higher pressures and temperatures builds the main component of many white dwarf stars [6]. In addition, solid carbon samples are rapidly heated during many laboratory applications and experiments [7–9]. A premier example is inertial confinement fusion experiments where carbon is one of the candidates for the ablator material [10]. Again, melting and the equation of state at high pressures are of crucial importance for precise modeling.

Driven by the applications in astrophysics and fusion research, carbon at high pressure was investigated by several theoretical approaches and simulation techniques. However, the predictions for the phase boundaries, in particular, the slope of the melting line, disagree between studies. The majority of differences results from the fact that the microscopic structures of the solid and liquid states close to the phase transition remain poorly understood [11–13]. To date, only a few measurements of macroscopic melting properties exist [8,9,14] while a direct probe of the microscopic structure in the sample that can discriminate between models has not been performed.

Compression and heating by strong shock waves is a standard technique to create the extreme states close to the melting line of carbon. While the shock-induced transition from graphite to diamond at ~20 GPa is now well understood [15], the subsequent melting is very difficult to diagnose due to its relatively small volume change [16]. In fact, the shock-induced graphite-liquid transition has not been determined reliably so far. At higher pressures, the melting of optically transparent diamond has been observed indirectly via changes in reflectivity and emitted radiation of the shock front [8,14]. However, optical properties are primarily determined by electronic states and, thus, are not necessarily connected to a new atomic structure. Other experiments, also using the shock compression of diamond, determined the phase transition from the small change in slope of the density-pressure curve [17,18]. In the present study, we combine the creation of liquid carbon by a laser-driven shock with the direct probing of the resulting atomic structure in the sample via spectrally resolved x-ray scattering. For the first time, the direct measurement of the microscopic ion structure of liquid carbon will thus allow us to discriminate between different theoretical models.

The experiments (see Fig. 1) were carried out at the GSI Helmholtzzentrum für Schwerionenforschung GmbH. The nhelix laser system (65 J, 11 ns, 1064 nm, 250 μm focal spot) was used to drive shock waves into porous, polycrystalline graphite with an initial density of 1.84 g/cm^3. The shock transit times were measured by an optical streak camera recording the self-emission of the shock release [19]. The expansion velocity of the latter can be used to determine the particle velocity applying the doubling rule [20]. The expansion velocity of the shock release was measured by a multiframe shadowgraphy instrument [21].

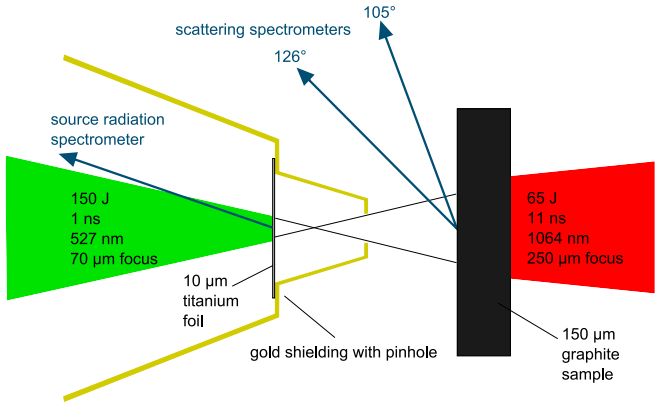

FIG. 1 (color online). Schematic of the experimental setup. The laser which is incident from the right onto the graphite sample drives the shock wave to create the investigated state of matter. Another laser with a significantly smaller pulse duration but higher energy creates a bright x-ray source of titanium-helium-alpha radiation at 4.75 keV which is collimated by a pinhole for probing the interesting regions of the sample. The x-ray source radiation and scattered radiation are monitored and spectrally resolved by HOPG spectrometers.

Density and pressure behind the shock front were then deduced by using the Rankine-Hugoniot relations [22]. The compressed material is found to have a mass density of 3.9 ± 0.2 g/cm^3 and a pressure of 147 ± 17 GPa. Applying a slightly larger focal spot of the driving laser, fluid carbon with a pressure of 86 ± 11 GPa and a mass density of 3.9 ± 0.2 g/cm^3 has been achieved (see the Supplemental Material [23] for a more detailed description of the shock measurements).

The temporal evolution of the laser-driven sample was simulated using the radiative-hydrodynamic code MULTI2D [24] in combination with the SESAME equation of state. The simulations predict a mass density of 3.8 g/cm^3, a temperature of ~8000 K, and a pressure of 150 GPa behind the shock front. These results are in very good agreement with both velocity measurements and multi-frame imaging of the shock release. As shown in Fig. 2, the obtained results clearly indicate that the thermodynamic parameters of the sample are homogeneous within 10% or better inside the channel probed by the x rays, and a well-defined state is probed in our experiments.

The microscopic structure of the exotic states created by the shock wave was investigated by spectrally resolved x-ray scattering [25]. The PHELIX laser system (150 J, 1 ns, 527 nm, 70 μm focal spot) was used to illuminate a titanium foil placed 500 μm from the rear surface of the carbon sample. The resulting hot plasma is a source for titanium-helium-alpha radiation at 4.75 keV and emits around 10^{15} photons into the whole solid angle. The source radiation was measured by a highly oriented pyrolytic graphite (HOPG) spectrometer for each laser shot. To probe the homogeneous region in the sample only, the x rays were collimated by a 110 μm pinhole which was incorporated into a gold cone structure to ensure sufficient shielding. The scattered photons are collected at different angles in backscattering geometry by two spectrometers using curved HOPG crystals in von Hamos geometry and image plates as detectors. The corresponding wave number changes of the scattered photons are $k = 3.8$ Å^{-1} (105°) and $k = 4.3$ Å^{-1} (126°). These wave numbers were chosen in order to have sensitive measurements of the predicted atomic structure in carbon and are thus very sensitive to the phase transition.

The scattered radiation power per solid angle is given by [26]

$$\frac{dP}{d\Omega} = I_0 r_0^2 \frac{1}{2}[1 + \cos^2\theta] N S(k), \tag{1}$$

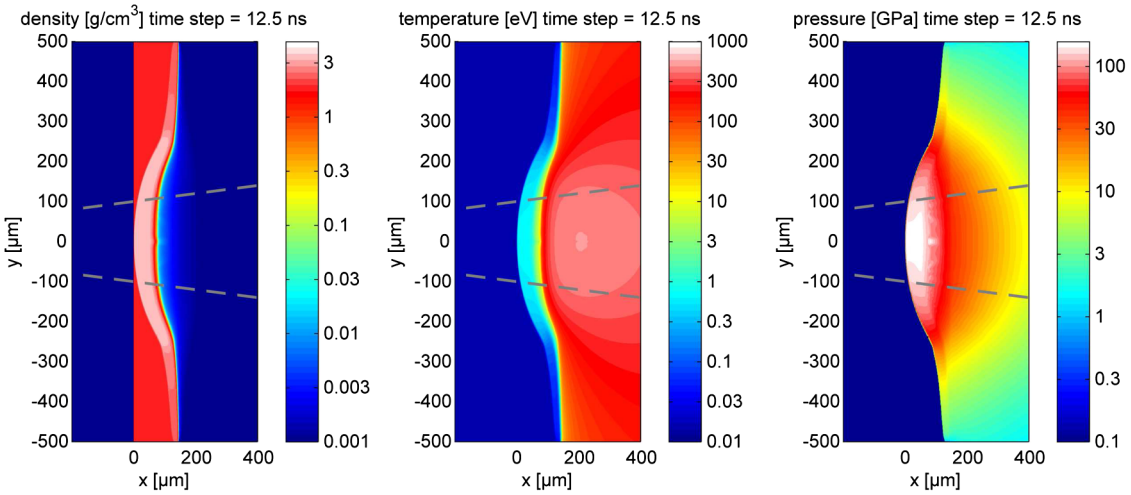

FIG. 2 (color online). MULTI2D hydrodynamic simulations of the shock-compressed graphite sample. At 12.5 ns after the drive laser impact, the shock wave reaches the sample rear side. Density, temperature, and pressure inside the shock wave are sufficiently homogeneous within the channel, which is probed by the x rays (indicated by the dashed gray lines).

where I_0 is the initial probe intensity, r_0 the classical electron radius, θ the scattering angle, and N the number of atoms in the probe volume. $S(k)$ denotes the frequency-integrated electron structure factor which contains all the information of the ion structure in the sample. For the backscattering geometry used here and assuming low ionization, it can be decomposed into two terms [27,28],

$$S(k) = |f(k)|^2 S_{ii}(k) + \sum_{n=1}^{Z_{wb}} [1 - f_n(k)^2]. \quad (2)$$

The first term describes elastic scattering which is mainly dominated by scattering from tightly bound electrons: $f(k)$ is the atomic form factor including all bound electrons, and $S_{ii}(k)$ is the structure factor of the nuclei. The second term accounts for the inelastic scattering from Z_{wb} weakly bound electrons with the corresponding form factors $f_n(k)$ of these electrons. As the form factors are known, a measurement of the (frequency-integrated) strength of the elastic and inelastic scattering features provides direct information about the atomic structure,

$$S_{ii}(k) = \frac{1}{|f(k)|^2}\left[\sum_{n=1}^{Z_{wb}} [1 - f_n^2(k)]\right]\frac{x_{el}}{x_{inel}}. \quad (3)$$

Here, we introduced the intensities of elastically and inelastically scattered radiation x_{el} and x_{inel}, respectively. Since $S_{ii}(k)$ only depends on the ratio of these quantities, no absolutely calibrated detector is required here.

A sample spectrum obtained by the HOPG spectrometer at a 126° scattering angle is shown in Fig. 3, where the different scattering features can clearly be identified. The elastic feature displays the spectral distribution of the helium-alpha line from the laser-driven titanium source. The inelastic feature results from a convolution of the source spectrum with the Compton profile for the weakly bound electrons [29]. Combining the measured x-ray source spectrum, the known bound-free Compton profile with the weight contained in both features gives the atomic structure $S_{ii}(k)$ via Eq. (3). For the scattering angle of 126°, we obtain $S_{ii} = 0.82 \pm 0.07$ for the structure factor.

Using the method described above, the structural changes induced by the shock wave can be determined for all angles or wave numbers and times where spectrally resolved scattering spectra have been recorded. Figure 4 shows the temporal evolution of the structure factor for a scattering angle of 126°. For cold graphite, the structure at this angle is close to zero, as the Bragg reflection of the (0 1 3) plane is only marginally covered by the spectrometer. Contrarily, there is a strong increase of the structure factor up to the time of shock release if the sample is driven into the fluid phase. This behavior can be explained by the geometry of the setup: as the probe radiation enters the sample from the opposite side than the shock drive, the attenuation of both the incident and the scattered photons is less for parts of the sample that get shocked at later times. Accordingly, the signal rises stronger than the volume of shocked material (linear increase). Moreover, absorption also reduces contributions from the hot plasma with direct laser illumination to less than 5%. The recorded rise of the atomic structure factor is thus a good representation of the structural changes to a fluid. It can be modeled well by a fixed ratio of the structure factors of cold solid and shocked material. At times after the shock release, the rarefaction creates a gaslike state which is best described by a structure factor of $S_{ii} = 1$.

The obtained values for the atomic structure factor are well suited to distinguish between different theoretical predictions and also avoid regions where solid parts may alter the results through Bragg reflections. As shown in Fig. 5, the region covered by the two scattering angles is

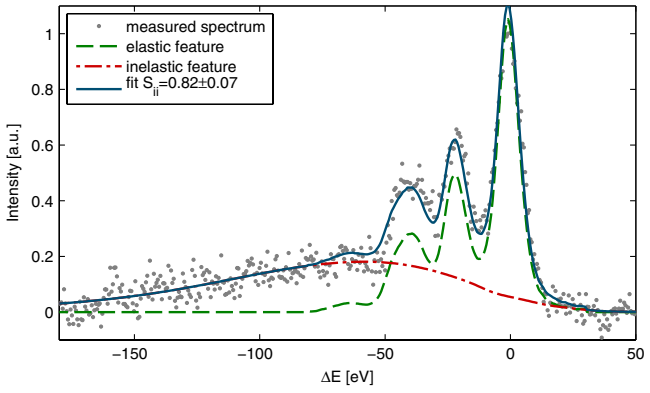

FIG. 3 (color online). Example of the x-ray scattering spectrum for $\theta = 126°/k = 4.3$ Å^{-1} used to extract the atomic structure. The elastic feature (dashed green line) represents the spectral distribution of the titanium-helium-alpha source radiation. The inelastic feature (dash-dotted red line) is given by the convolution of the source spectrum and a Compton profile for the weakly bound electrons. Combining the two features yields the structure factor as the only free parameter.

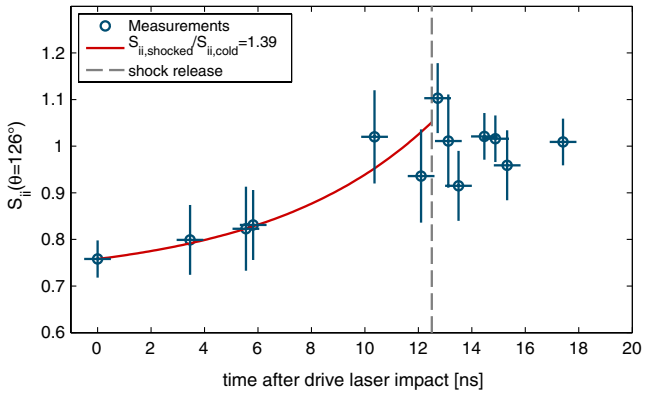

FIG. 4 (color online). Time evolution of the extracted structure factor at $k = 4.3$ Å^{-1} ($\theta = 126°$). During the shock wave propagation, the increase can be explained by a fixed ratio of the structure value between cold and shocked materials. After the shock release, the rarefaction creates a gaslike state with $S_{ii}(k) = 1$.

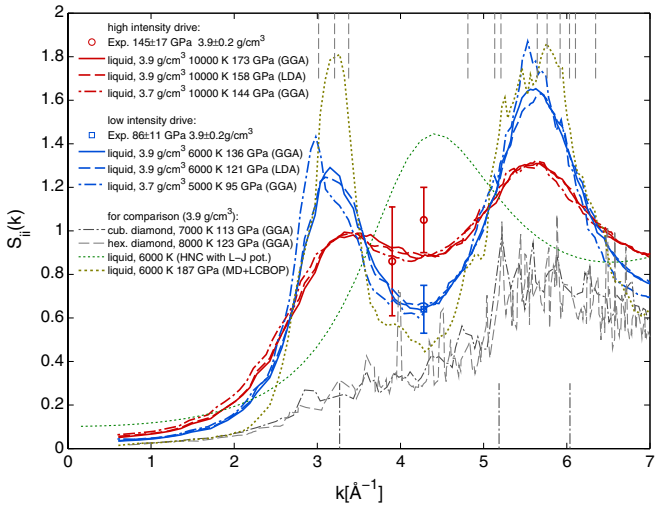

FIG. 5 (color online). Comparison of the obtained atomic structure with *ab initio* DFT-MD simulations of carbon phases which might be present inside the sample: cubic diamond, hexagonal diamond, or liquid carbon. For a clearer view, the Bragg maxima of the crystalline solid phases are indicated by short lines at the top and bottom. For the low-pressure case, the sample is very close to the solid-fluid phase boundary. For comparison, we show a structure factor obtained using a Lennard-Jones 12-6 potential with an adjusted location of the minimum [hypernetted chain (HNC) with a Lennard-Jones potential] and results from classical MD simulations using a more complex LCBOP potential [33].

free of Bragg peaks from the hexagonal and cubic diamond phases at high pressures. To include thermal excitations, we have investigated these phases with density functional theory molecular dynamics (DFT-MD) simulations at finite temperatures (see the Supplemental Material [23]). The simulations give well-defined peaks as well as a diffusive background which is, however, well below the measured structure factors. In agreement with the hydrodynamics simulations and other equation of state models, we thus can conclude that the sample was driven into the fluid phase. To reproduce the recorded pressure in the simulations, the density was varied within the experimental error. Moreover, different approaches for the exchange-correlation term in DFT have been used: the generalized gradient approximation (GGA) and the local density approximation (LDA). These variations do not change the structure significantly but influence the resulting pressure. For the high intensity drive, reducing the density to 3.7 g/cm^3 or using LDA has the same effect and brings the pressure in line with the experimental result. For the low intensity drive, only the reduced density case completely matches the pressures from the experiment.

The fluid phase for carbon is far from being a simple liquid. DFT-MD simulations predict a structure that is complex and shows signs of short-lived chemical bonding [30,31]. Figure 5 illustrates that simple, purely repulsive pair interactions as known from plasma theories cannot describe the observed data. Simple potentials from fluid theory like that of Lennard and Jones fail as well. We have also tested combinations of screened Coulomb interactions and Lennard-Jones-type interactions. All of these calculations always predict a first peak around $k = 4.3$ Å^{-1} or a correlation length of 1.45 Å which is related to the mean density of the sample [32]. However, the measured data do not support such a structure factor. On the other hand, the observed structure factors agree very well with results from DFT-MD simulations. Such simulations include the full quantum nature of the electrons and, thus, go far beyond simple pair interactions between the nuclei. In particular, they are able to describe short-time bonding. Of course, such bonds play a larger role for colder systems, and, indeed, our data show that the experiment using a weaker shock (reduced drive) shows a much smaller structure factor between two well-pronounced peaks. The simulations also indicate that this case is very close to the melting line of carbon.

There exist more sophisticated approaches of a two-particle interaction potential for carbon which include many-particle effects. Our comparisons using a long-range carbon bond-order potential (LCBOP) [33] show principle agreement of the resulting structure with DFT-MD. However, this potential appears to be too stiff. Compared to DFT-MD, we find a higher pressure and a more pronounced structure which is not found in the experiment. Better agreement is expected for improved versions like LCBOPII [34,35].

Using spectrally resolved x-ray scattering from shock-compressed carbon, we are able to provide for the first time direct measurements of the atomic structure of liquid carbon in the 100 GPa regime. Our measurements confirm the complex structure predicted by quantum simulations and rule out simple pair interactions. Moreover, the method applied can also be used to determine phase transitions in such extreme conditions and can be used to constrain models of the carbon phase diagram in future experiments.

We thank the PHELIX team at GSI for their assistance. The work of D. K., A. O., and M. R. was supported by the BMBF, Support Code No. 06DA9043I.

[1] W. B. Hubbard, W. J. Nellis, A. C. Mitchell, N. C. Holmes, S. S. Limaye, and P. C. McCandless, Science **253**, 648 (1991).
[2] S. Stanley and J. Bloxham, Nature (London) **428**, 151 (2004).
[3] M. Ross, Nature (London) **292**, 435 (1981).
[4] B. L. Sherman, H. F. Wilson, D. Weeraratne, and B. Militzer, Phys. Rev. B **86**, 224113 (2012).
[5] N. Madhusudhan, K. K. M. Lee, and O. Mousis, Astrophys. J. Lett. **759**, L40 (2012).
[6] P. Dufour, J. Liebert, G. Fontaine, and N. Behara, Nature (London) **450**, 522 (2007).

[7] J. Zazula, LHC Project Note No. 78, 1997.
[8] J. H. Eggert, D. G. Hicks, P. M. Celliers, D. K. Bradley, R. S. McWilliams, R. Jeanloz, J. E. Miller, T. R. Boehly, and G. W. Collins, Nat. Phys. **6**, 40 (2010).
[9] A. Pelka *et al.*, Phys. Rev. Lett. **105**, 265701 (2010).
[10] J. D. Lindl, P. Amendt, R. L. Berger, S. G. Glendinning, S. H. Glenzer, S. W. Haan, R. L. Kauffman, O. L. Landen, and L. J. Suter, Phys. Plasmas **11**, 339 (2004).
[11] M. P. Grumbach and R. M. Martin, Phys. Rev. B **54**, 15 730 (1996).
[12] A. I. Savvatimskiy, Carbon **43**, 1115 (2005).
[13] A. A. Correa, L. X. Benedict, D. A. Young, E. Schwegler, and S. A. Bonev, Phys. Rev. B **78**, 024101 (2008).
[14] D. K. Bradley, J. H. Eggert, D. G. Hicks, P. M. Celliers, S. J. Moon, R. C. Cauble, and G. W. Collins, Phys. Rev. Lett. **93**, 195506 (2004).
[15] D. J. Erskine and W. J. Nellis, Nature (London) **349**, 317 (1991).
[16] X. Wang, S. Scandolo, and R. Car, Phys. Rev. Lett. **95**, 185701 (2005).
[17] D. G. Hicks, T. R. Boehly, P. M. Celliers, D. K. Bradley, J. H. Eggert, R. S. McWilliams, R. Jeanloz, and G. W. Collins, Phys. Rev. B **78**, 174102 (2008).
[18] M. D. Knudson, M. P. Desjarlais, and D. H. Dolan, Science **322**, 1822 (2008).
[19] D. Kraus *et al.*, High Energy Density Phys. **8**, 46 (2012).
[20] A. Benuzzi-Mounaix *et al.*, Phys. Plasmas **9**, 2466 (2002).
[21] M. Börner *et al.*, Rev. Sci. Instrum. **83**, 043501 (2012).
[22] Y. B. Zeldovic and Y. P. Raizer, *Physics of Shock Waves and High-Temperature Hydrodynamic Phenomena* (Academic, New York, 1966).
[23] See Supplemental Material http://link.aps.org/supplemental/10.1103/PhysRevLett.111.255501 for further details on the shock measurements and DFT-MD calculations.
[24] R. Ramis, J. Meyer-ter-Vehn, and J. Ramires, Comput. Phys. Commun. **180**, 977 (2009).
[25] S. H. Glenzer and R. Redmer, Rev. Mod. Phys. **81**, 1625 (2009).
[26] J. Sheffield, D. Froula, S. H. Glenzer, and N. C. Luhmann, *Plasma Scattering of Electromagnetic Radiation* (Academic, New York, 2010), 2nd ed.
[27] J. Chihara, J. Phys. Condens. Matter **12**, 231 (2000).
[28] R. James, *The Optical Principals of the Diffraction of X-Rays* (Ox Bow Press, London, 1962).
[29] M. Schumacher, F. Smend, and I. Borchert, J. Phys. B **8**, 1428 (1975).
[30] J. N. Glosli and F. H. Ree, Phys. Rev. Lett. **82**, 4659 (1999).
[31] J. Vorberger and D. O. Gericke, High Energy Density Phys. **9**, 178 (2013).
[32] T. Ma *et al.*, Phys. Rev. Lett. **110**, 065001 (2013).
[33] J. H. Los and A. Fasolino, Phys. Rev. B **68**, 024107 (2003).
[34] J. H. Los, L. M. Ghiringhelli, E. J. Meijer, and A. Fasolino, Phys. Rev. B **72**, 214102 (2005).
[35] L. M. Ghiringhelli, J. H. Los, A. Fasolino, and E. J. Meijer, Phys. Rev. B **72**, 214103 (2005).